GDCh

Minireviews

Angewandte
Chemie
International Edition
www.angewandte.org

Check for updates

Locally Concentrated Ionic Liquid Electrolytes for Lithium-Metal Batteries

Xu Liu, Alessandro Mariani, Henry Adenusi, and Stefano Passerini*
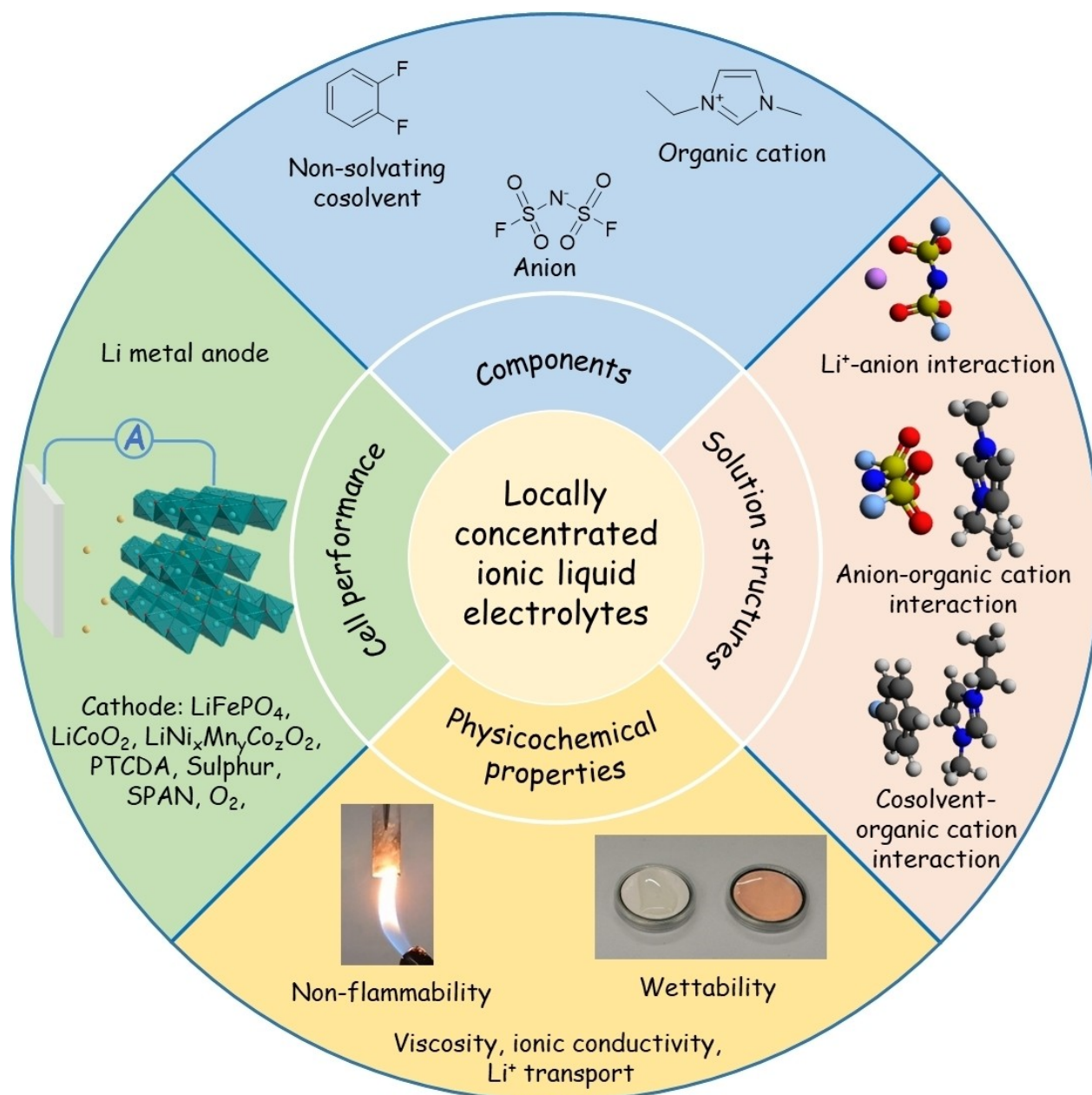
Abstract: Non-flammable ionic liquid electrolytes (ILEs) are well-known candidates for safer and long-lifespan lithium metal batteries (LMBs). However, the high viscosity and insufficient Li$^+$ transport limit their practical application. Recently, non-solvating and low-viscosity co-solvents diluting ILEs without affecting the local Li$^+$ solvation structure are employed to solve these problems. The diluted electrolytes, i.e., locally concentrated ionic liquid electrolytes (LCILEs), exhibiting lower viscosity, faster Li$^+$ transport, and enhanced compatibility toward lithium metal anodes, are feasible options for the next-generation high-energy-density LMBs. Herein, the progress of the recently developed LCILEs are summarised, including their physicochemical properties, solution structures, and applications in LMBs with a variety of high-energy cathode materials. Lastly, a perspective on the future research directions of LCILEs to further understanding and achieve improved cell performances is outlined.

1. Introduction

Li metal, with a high theoretical capacity (3860 mAh g^{-1}, 2061 mAh cm^{-3}) and the most negative redox potential (-3.04 V vs. SHE), is a promising anode material for the next-generation high-energy-density batteries, i.e., lithium metal batteries (LMBs).[1] However, the lack of sufficiently protective solid electrolyte interphases (SEIs) on lithium metal anodes (LMAs) leads to low lithium stripping/plating Coulombic efficiency (CE) and lithium dendrite growth, which limits the lifespan of LMBs.[2,3] Moreover, the heat generation from the side reactions and internal short circuit, together with the conventionally used flammable electrolytes, result in safety concerns.[4,5] Among the strategies proposed to mitigate these issues, modulating the electrolyte design by selecting specific electrolyte components and adjusting their concentrations have been considered the most relevant, as it can tune the SEI formation, lithium deposition morphology, and electrolyte flammability.[6,7]

Ionic liquid electrolytes (ILEs), i.e., mixtures of lithium salts and ionic liquids (ILs) consisting of bulky organic cations and anions, are well-known candidates for high-safety and long-lifespan LMBs.[8,9] A subclass of ILEs can be chosen from specific organic cations and anions that exhibit non-volatility and high thermal stability, greatly reducing the flammability for the corresponding ILE, thus enhancing the safety profile for high-energy applications.[10] The SEIs derived from the organic cations and anions allow stable cycling of LMAs.[11–13] Moreover, the chemical diversities of the organic cations and anions offer multifarious choices of the ILEs enabling highly reversible LMBs with different high-energy cathode materials, e.g., Ni-rich layered/spinel oxides,[14,15] lithium-rich oxides,[16] cation-disordered rock-salt oxides,[17] sulphur,[18] and even oxygen.[19]

Nevertheless, the insufficient Li$^+$ transport and high viscosity of the conventionally used ILEs with lithium salt mole percent of $\approx$10–20% limit the operation of LMBs under practical conditions of high current density, e.g., 0.5 mA cm^{-2}, and high mass loading cathodes, e.g., 10 mg cm^{-2}, at room temperature (RT).[14,20] Despite the increased electrolyte viscosity, concentrated ionic liquid electrolytes (CILEs) containing higher lithium salt mole percent ($\approx$30–50%) are reported to allow the operation of LMBs at higher dis-/charge rates, which results from higher Li$^+$ concentrations and improved Li$^+$ transference numbers caused by fewer organic cations and free anions.[21–24] Even though, the rate capability delivered with such CILEs is still inferior to those with conventional carbonate-based electrolytes,[16,22] due to the sluggish Li$^+$ mobility limited by the high viscosity. Moreover, the increased viscosity of the CILEs caused by the elevated formation of Li$^+$-anion complexes severely hampers the wettability toward thick electrodes.

The addition of low-viscosity co-solvents is an effective strategy to mitigate the high viscosity and sluggish Li$^+$ mobility of ILEs.[25–28] However, the early adopted co-solvents are involved in the Li$^+$ solvation and/or are unstable towards LMAs. Their coordination with Li$^+$ releases more free anions, which decreases the Li$^+$ transference number and therefore, lead to unsatisfying rate capability at RT.[26,27] The instability of the co-solvent, e.g., dimethyl carbonate (DMC), towards LMAs lowers lithium stripping/plating CEs, particularly when they are involved in Li$^+$ solvation.[29,30]

Recently, non-solvating fluorinated ethers and aromatic molecules have been employed as new co-solvents to resolve the aforementioned issues,[30,31] which is inspired by a similar approach for concentrated electrolytes based on conventional organic solvents.[32–40] The strong electron-withdrawing effect of the fluorinated groups weakens the solvating ability of the co-solvents towards Li$^+$, and the consequent non-solvating feature allows the dilution of CILEs with the local Li$^+$ coordination and elevated Li$^+$ transference number preserved.[29–31,41–44] The non-solvating co-solvents could

[*]   Dr. X. Liu, Dr. A. Mariani, Prof. Dr. S. Passerini
      Helmholtz Institute Ulm (HIU)
      Helmholtzstraße 11, 89081 Ulm (Germany)
      Karlsruhe Institute of Technology (KIT)
      P.O. Box 3640, 76021 UlmKarlsruhe (Germany)
      E-mail: stefano.passerini@kit.edu

      Dr. H. Adenusi
      Hong Kong Quantum AI Lab
      17 Science Park West Avenue, Hong Kong (China)

      Prof. Dr. S. Passerini
      Chemistry Department, Sapienza University
      Piazzale A. Moro 5, 00185 Rome (Italy)

      Dr. A. Mariani
      Present address: ELETTRA Synchrotron of Trieste
      34012 Basovizza, Trieste (Italy)

promote the formation of more protective SEIs kinetically enhancing the stability of LMAs against the electrolytes.[30,31,41,45,46] As a result, the Li$^+$ transport and fluidity of CILEs are promoted without compromising the CE of Li stripping/plating.[29–31,41–43,45,46] Electrolytes consisting of CILEs and the non-solvating co-solvents are named as locally concentrated ionic liquid electrolytes (LCILEs).

Compared with the locally concentrated electrolytes based on conventional organic solvents, e.g., carbonate esters,[40] ethers,[39] sulfones,[47] and phosphate esters,[34] LCILEs exhibit lower flammability and better compatibility toward LMAs.[31,45,48] On the other hand, the interaction of the positively charged organic cations with the other species in LCILEs is different from that of molecular, i.e., neutral, organic solvents in their locally concentrated electrolytes,[49–51] requiring extra attention for the design of LCILEs. Up to now, several rationally designed LCILEs with thoroughly improved Li$^+$ transport and decreased viscosity have been developed, allowing stable cycling of LMBs with high-mass-loading insertion-type cathodes, lithium-sulfur (Li–S) batteries, and lithium-oxygen (Li-O$_2$) batteries at elevated current densities.[30,31,42,45,46,52] Despite the remarkable progress and ever increasing attention, the research on LCILEs has not been reviewed to the best of our knowledge.

Herein, this minireview summarises the recent progress of LCILEs to promote their further development for high-energy-density LMBs. Firstly, the influence of the non-solvating co-solvents on LCILEs' physicochemical proper-

ties that are critical for practical application is introduced. The ion-ion and ion-diluent interactions associated with the physicochemical properties in LCILEs are then classified and presented. The progress of LCILEs designed for LMAs and a few specific cathodes is also summarised. Lastly, a comment and perspective on future research directions is presented. The names and acronyms which will be used in this review for the organic cations, anions, and non-solvating co-solvents of the reported LCILEs are shown in Table 1 along with their respective chemical structure shown in Figure 1.

2. Influence of non-solvating co-solvents on the physicochemical properties

2.1. Flammability

Non-flammability is one of the most important properties of ILEs for safer LMBs. The ignition test is the most used method to evaluate the flammability of electrolytes. Lee et al. reported that both the separator soaked with CILE ([LiTFSI]$_1$[Pyr$_{13}$FSI]$_2$) and LCILE ([LiTFSI]$_1$[Pyr$_{13}$FSI]$_2$-[TTE]$_2$) could not be ignited by flame torch (Figure 2a), indicating the nonflammability.[30] Wang et al. also demonstrated the non-flammability of a LCILE ([LiFSI]$_1$-[Pip$_{13}$FSI]$_2$[TTE]$_4$) containing 52.7 wt.% TTE via a similar ignition test.[41]

Xu Liu obtained his master degree in 2017 from Yunnan University under the supervision of Prof. Yude Wang, and obtained his PhD in 2021 from the Helmholtz-Institute Ulm (HIU) of the Karlsruhe Institute for Technology (KIT) under the supervision of Prof. Stefano Passerini. He is currently working as a postdoctoral researcher at HIU/KIT. His research activities are focused on electrolytes for high-energy batteries, particularly those based on ionic liquids.

Alessandro Mariani received his PhD in Physical Chemistry in 2016 at La Sapienza University of Rome (Italy). He then spent 2 years as a Postdoc at the European Synchrotron Radiation Facility (ESRF, Grenoble, France) on the ID02 TRUSWAXS beamline, serving as local contact for external users and focusing on the liquid-liquid phase transition of complex systems. In 2018, he moved to the Helmholtz Institute Ulm, where he started working on electrolytes for batteries. He is now co-responsible for the SAXS beamline at the italian synchrotron Elettra. He is an expert in the use of SAXS, Raman and NMR spectroscopies, and MD and DFT simulations.

Henry Adenusi completed his PhD at Sapienza University of Rome; he was awarded the 'Vito Volterra' International Fellowship. Currently, he is a Postdoctoral Fellow at the Hong Kong Quantum AI Lab, joint centre of The University of Hong Kong (HKU) and the California Institute of Technology (Caltech) working on the AI & quantum mechanical simulation platform for next generation materials discovery. Research focus is on merging computational simulations with electrochemistry experiments and AI technologies (machine learning) for battery materials.

Stefano Passerini is Professor at the Chemistry Department of Sapienza University of Rome. Formerly professor at the Karlsruhe Institute of Technology, Helmholtz Institute Ulm (Germany) and the University of Muenster (Germany), he cofounded the MEET battery research center. His research focuses on the basic understanding and development of materials for high-energy batteries and supercapacitors, with the goal to create sustainable energy storage systems from environmentally friendly and available materials and processes. He is an internationally recognized pioneer in the field of ionic liquids and the development of alkali-ion batteries.

Table 1: . Names and acronyms of the organic cations, anions, and non-solvating co-solvents of the reported LCILEs.

Types	Acronyms	Names
Organic cations	Pyr_{13}^+	N-methyl-N-propylpyrrolidinium cation
	Pyr_{14}^+	N-butyl-N-methylpyrrolidinium cation
	Pyr_{1201}^+	N-methoxyethyl-N-methylpyrrolidinium cation
	Pyr_{120201}^+	N-(2-(2-methoxyethoxy)ethyl)-N-methylpyrrolidinium cation
	$Pyr_{1(20)71}^+$	N-methyl-N-oligo(ethylene oxide)pyrrolidinium cation (7 repeated ethylene oxide unit)
	$DEME^+$	N,N-diethyl-N-(2-methoxyethyl)-N-methylammonium cation
	Pip_{13}^+	N-methyl-N-propylpiperidinium cation
	$Emim^+$	1-ethyl-3-methylimidazolium cation
Anions	FSI^-	bis(fluorosulfonyl)imide anion
	$TFSI^-$	bis(trifluoromethanesulfonyl)imide anion
Co-solvents	BTFE	bis(2,2,2-trifluoroethyl) ether
	TTE	1,1,2,2-tetrafluoroethyl 2,2,3,3-tetrafluoropropyl ether
	OTF	1H,1H,5H-octafluoropentyl 1,1,2,2-tetrafluoroethyl ether
	dFBn	1,2-difluorobenzene
	mFBn	monofluorobenzene
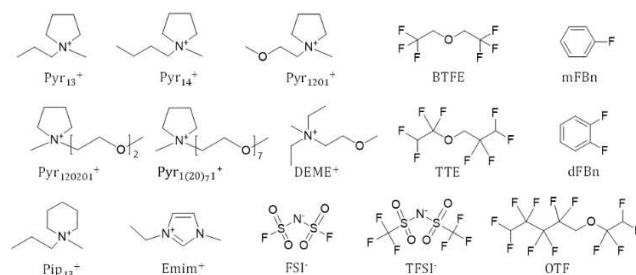
Figure 1. The chemical structure of the organic cations, anions, and non-solvating co-solvents of the reported LCILEs.
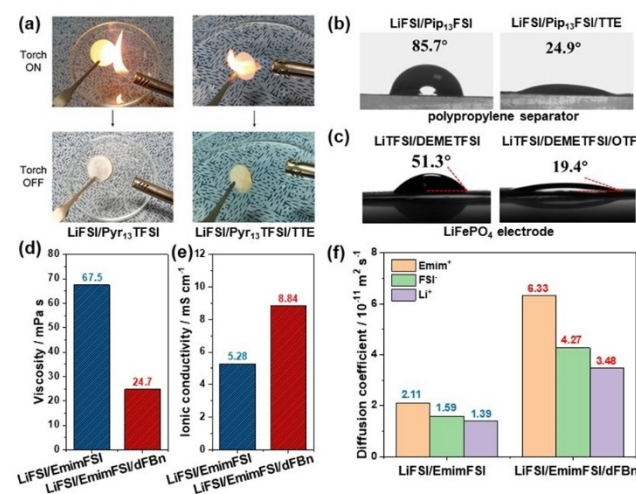
Figure 2. (a) Ignition tests of $[LiTFSI]_1[Pyr_{13}FSI]_2$ and $[LiTFSI]_1[Pyr_{13}FSI]_2[TTE]_2$ (reproduced from Ref. [30]). (b) Wettability of $[LiFSI]_1[Pip_{13}FSI]_2$ and $[LiFSI]_1[Pip_{13}FSI]_2[TTE]_4$ toward polypropylene separator (reproduced from Ref. [41]). (c) Wettability of $[LiTFSI]_{0.8}[DEMETFSI]_1$ and $[LiTFSI]_{0.8}[DEMETFSI]_1[OTF]_4$ toward LiFePO$_4$ electrode (reproduced from Ref. [42]). (d) Viscosity, (e) ionic conductivity, and (f) self-diffusion coefficients obtained with pulsed-field gradient nuclear magnetic resonance (PFG NMR) of $[LiFSI]_1[EmimFSI]_2$ and $[LiFSI]_1[EmimFSI]_2[dFBn]_2$ at 20°C (reproduced from Ref. [31]).

Apart from the qualitative ignition tests, more precise determination of the flammability is given by the flashpoint tests. The American Occupational Safety and Health Standards defines that any liquid having a flashpoint at or below

93°C is a flammable liquid.[53] The occurrence of a flash requires enough vapour of the combustible liquids to be mixed with air for ignition. ILEs exhibit nearly zero vapour pressure, so a flash does not occur during the tests of their flashpoints, i.e., ILEs are non-flammable liquids. On the contrary, most of the co-solvents of the reported LCILEs exhibit flashpoints much lower than 93°C. According to the suppliers, the flashpoints of TTE, BTFE, OTF, dFBn, and mFBn are 27.5, 1.0, 45.0, 1.0, and −12.0°C, respectively. Surprisingly, despite the high content of flammable BTFE (around 30 wt.%), no flash was detected for $[LiFSI]_1$-$[EmimFSI]_2[BTFE]_2$ and $[LiFSI]_1[Pyr_{14}FSI]_2[BTFE]_2$ in the temperature range of 25–300°C.[48] But this is not the case for all the LCILEs. For example, the flashpoints of $[LiFSI]_1$-$[EmimFSI]_2[mFBn]_2$ containing only 20 wt.% of flammable co-solvents was determined to be 98°C. This value is still above the threshold flashpoint (93°C) for flammable liquids, so this LCILE is still classified as a non-flammable liquid.[45] But the occurrence of the flash indicates the necessity of flashpoint measurements to assess the flammability of the developed LCILEs.

2.2. Wettability towards separators and electrodes

The most promising ILEs for LMBs usually employ FSI⁻ and/or TFSI⁻ anions, but these electrolytes exhibit poor wettability towards the commercially available separators based on polyolefin, e.g., polyethylene (PE) and/or polypropylene (PP).[54,55] The separators used for the early investigation of ILEs for LMBs were mostly made of glass fibre with large pores, leading to the formation of porous lithium depositions that easily penetrate across the porous separator and cause short circuit.[29,54]

It is demonstrated that such an issue is effectively solved when the non-solvating co-solvents are introduced to ILEs. For example, Wang et al. reported that the contact angles of $[LiFSI]_1[Pip_{13}FSI]_2$ and $[LiFSI]_1[Pip_{13}FSI]_2[TTE]_4$ on commercial PP separators were 85.7° and 24.9°, respectively (Figure 2b).[41] The improved wettability has been also reported for TFSI⁻-based LCILEs and PE separators.[30] The use of the well-wetted commercial polyolefin separators with more uniform micro-pores benefits the reported long-term dendrite-free cycling of LMAs in LCILEs.

In addition, the wettability toward electrodes is also promoted possibly due to the decreased electrolyte viscosity in the presence of low-viscosity diluents. For example, Cai et al. reported that the contact angle of $[LiTFSI]_{0.8}$-$[DEMETFSI]_1[OTF]_4$ and $[LiTFSI]_{0.8}[DEMETFSI]_1$ on LiFePO$_4$ electrodes were 51.3° and 19.4° (Figure 2c),[42] respectively, which is relevant for the use of thick electrodes.

2.3. Viscosity and ion transport

The viscosity of CILEs is effectively decreased when low-viscosity co-solvents are added. For example, the viscosity of $[LiFSI]_1[EmimFSI]_2$ at 20°C is 67.5 mPa s, which decreases

to 24.7 mPa s for [LiFSI]$_1$[EmimFSI]$_2$[dFBn]$_2$ containing 22.9 wt.% dFBn (Figure 2d).[31] Moreover, a higher mole fraction of the co-solvent leads to even lower viscosities. Nonetheless, it is not possible to indefinitely add a non-solvating co-solvent to a CILE, differently from the solvating co-solvents which are miscible with ILEs.[28] The systems based on non-solvating co-solvent tend to reach a saturation concentration, and further addition of the co-solvent will lead to a liquid-liquid phase separation.[29,43] Among the currently reported LCILEs, [LiFSI]$_1$[Pip$_{13}$FSI]$_2$[TTE]$_4$ exhibits the lowest viscosity of 6.8 mPa s,[41] which is comparable to conventional carbonate electrolytes for LIBs.

The room-temperature ionic conductivity of CILEs, fully consisting of ions, is mainly limited by the high viscosity. The decreased viscosity due to the addition of non-solvating co-solvents to CILEs is accompanied with increased ionic conductivity. For example, the ionic conductivity of [LiFSI]$_1$-[EmimFSI]$_2$ and [LiFSI]$_1$[EmimFSI]$_2$[dFBn]$_2$ at 20°C is 5.28 and 8.84 mS cm^{-1} (Figure 2e), respectively.[31]

However, it should be noted that all the ionic species including Li$^+$, organic cations, and anions contribute to the ionic conductivity, while only the Li$^+$ transport accounts for the operation of the LMBs. To estimate the contribution of Li$^+$ transport to the ionic conductivity, i.e., the transference number of Li$^+$, the Bruce-Vincent method combining the DC polarisation and AC impedance of Li/Li symmetric cells are frequently used.[56] In general, the Li$^+$ transference number of LCILEs is not lower than the corresponding CILEs,[29,30,41,46] which, together with the higher ionic conductivity of the LCILEs, indicates a faster Li$^+$ mobility of LCILEs than the corresponding CILEs. Nonetheless, the interfacial resistance is one order of magnitude higher than the ohmic resistance in the reported AC impedance spectra for the measurement of Li$^+$ transference number,[29,30,41,46] which could lead to high deviation.

PFG NMR is also adopted to discriminate the contribution of the ions to the ionic conductivity. The self-diffusion coefficients of the ions in the electrolytes are directly obtained with PFG NMR, which already reflect the mobility of these ions. For instance, Figure 2d displays the measured self-diffusion coefficient of all the ionic charge carriers in [LiFSI]$_1$[EmimFSI]$_2$ and [LiFSI]$_1$[EmimFSI]$_2$[dFBn]$_2$.[31] All the ions exhibit higher self-diffusion coefficients in [LiFSI]$_1$-[EmimFSI]$_2$[dFBn]$_2$ than in [LiFSI]$_1$[EmimFSI]$_2$. The concerned Li$^+$ self-diffusion coefficient increases from 1.39×10^{-11} to 3.48×10^{-11} m^2 s^{-1}, proving the enhanced translational mobility of Li$^+$. Such improvements are also observed for other LCILEs.[30,45,48,57] With the mole fractions and the measured self-diffusion coefficients of the ionic charge carriers, the apparent Li$^+$ transference number can be calculated. The values for [LiFSI]$_1$[EmimFSI]$_2$ and [LiFSI]$_1$-[EmimFSI]$_2$[dFBn]$_2$ are 0.13 and 0.12, respectively.[31] Therefore, introducing the non-solvating co-solvents to LCILEs does not significantly affect the Li$^+$ transference number. Similar values and trends are also observed in several other CILEs and LCILEs.[30,31,45,48] However, the mole ratio of lithium salt to IL for these electrolytes is around 1:2. When this ratio changes, the transference number should be different. Since the non-solvating co-solvent has limited

influence on the Li$^+$ transference number, the enhanced ionic conductivity indicates the faster mobility of Li$^+$ in LCILEs with respect to the corresponding CILEs.

3. Ion-ion and ion-diluent interactions in LCILEs

3.1. Solvation of Li$^+$

The solvation structure of Li$^+$ is not only relevant to the physicochemical properties of the electrolyte but also the interfacial properties, e.g., desolvation process and SEI formation.[58-60] When a co-solvent is added to an ILE, the mixture will contain Li$^+$, organic cations, anions, and co-solvent molecules. Li$^+$ could be solvated by the other three species. For LCILEs, the co-solvents with poor coordination ability rarely coordinate to Li$^+$. Li$^+$ in LCILEs are mainly coordinated by anions and/or organic cations, depending on the structure of the organic cations.

3.1.1. LCILEs based on organic cations with purely alkyl side chains

The organic cations with purely alkyl side chains, e.g., Pyr$_{13}^+$, Pip$_{13}^+$, Pyr$_{14}^+$, and Emim$^+$ (Table 1, Figure 1), do not coordinate to Li$^+$, and the first solvation sheath of Li$^+$ in the LCILEs is governed by the negatively charged anions.[29-31,41,44,46,48,57,61]

Molecular dynamics (MD) simulations conducted on LCILEs based on this type of organic cations provide a physical picture of the solution structure.[31,41,45,48,61] Figure 3a shows a snapshot of the MD simulated box for [LiFSI]$_1$-[EmimFSI]$_2$[BTFE]$_2$.[48] The yellow spheres, red sticks, blue sticks, and cyan cloud represent Li$^+$, Emim$^+$, FSI$^-$, and BTFE, respectively. Most ions, including Li$^+$, FSI$^-$, and Emim$^+$, cluster to form ionic networks, which are distinguished from the BTFE micro domains containing no Li$^+$. Taking a close look at the ionic network, one can identify that Li$^+$ cations are directly coordinated by the FSI$^-$, which are further surrounded by the organic cations.

The Li$^+$ solvation sheath dominated by anions can be unravelled via radial distribution functions (RDFs), as illustrated for [LiFSI]$_1$[EmimFSI]$_2$[mFBn]$_2$ employing partially solvating mFBn as the co-solvent (Figure 3b).[45] Despite a minor peak at 2.22 Å for the Li–F(mFBn) curve, the first solvation shell of Li$^+$ is dominated by Li$^+$-FSI$^-$ coordination at 2.12 Å with respect to Li–O(FSI). On the other hand, although the interaction between Li$^+$ and the partially solvating mFBn is minor, it also affects the physicochemical properties of the electrolyte. When mFBn is replaced with the non-solvating dFBn, the coordination between Li$^+$ and the co-solvent in [LiFSI]$_1$[EmimFSI]$_2$[dFBn]$_2$ is almost diminished, which is accompanied by a decrease of ionic conductivity from 9.6 to 8.8 mS cm^{-1}, an increase of viscosity from 22 to 25 mPa s, and a slight increase of the Li$^+$ transference number from 0.118 to 0.120 at 20°C.[31,45] The former two have negative effects on Li$^+$ transport, while the latter is a positive effect. Therefore, the selection of co-
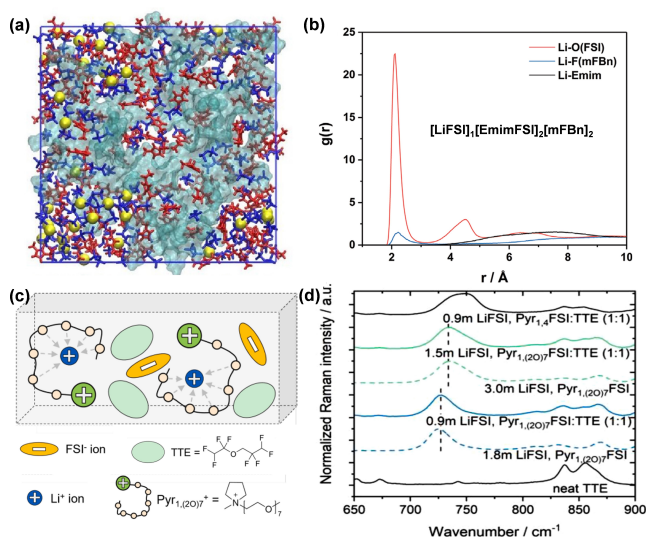
Figure 3. (a) Snapshots of the MD simulated box for [LiFSI]$_1$[EmimFSI]$_2$[BTFE]$_2$ (adapted from Ref. [48]). The yellow spheres, red sticks, blue sticks, and cyan clouds represent Li$^+$, Emim$^+$, FSI$^-$, and BTFE, respectively. (b) Radial distribution functions of Li–O(FSI), Li–F(mFBn), and Li-Emim pairs obtained from MD simulation of [LiFSI]$_1$[EmimFSI]$_2$[mFBn]$_2$ (adapted from Ref. [45]). (c) Schematic illustration of Li$^+$ coordination in LCILEs with solvating organic cation (Pyr$_{1(2O)71}$$^+$). (d) Raman spectra of N–S bond of FSI$^-$ in LCILEs employing either non-solvating Pyr$_{14}$$^+$ or solvating Pyr$_{1(2O)71}$$^+$. (c,d) adapted from Ref. [43].

solvents with rationally adjusted Li$^+$ solvation ability balancing the aforementioned opposite effects would lead to further optimised Li$^+$ transport ability.

3.1.2. LCILEs based on alkoxy-ether-functionalised organic cations

The alkyl side chains of the organic cations may be replaced with polar alkoxy-ethers. For example, DEME$^+$, Pyr$_{12O1}$$^+$, Pyr$_{12O2O1}$$^+$, and Pyr$_{1(2O)71}$$^+$ (shown in Table 1, Figure 1) belong to this type of organic cations.[42,43] The oxygen atoms with their lone-pairs in the alkoxy-ether side chain could coordinate to Li$^+$, which has been demonstrated in LiTFSI-Pyr$_{1(2O)x1}$TFSI (with $x = 1$, 2, 3, 4, and 7) binary ILEs.[62–65] Although Pyr$_{12O1}$$^+$ has already proven to have effects on the coordination environment of Li$^+$,[65] the Li$^+$ solvation is still mainly governed by TFSI$^-$.[62,65] With the strengthened coordination effect of the ether oxygen atoms for increased x, Li$^+$ tends to preferentially coordinate with the ether oxygen atoms rather than the anions.[62] For [LiTFSI]$_{0.15}$[Pyr$_{1(2O)21}$TFSI]$_{0.85}$, the Li$^+$ solvation is dominated by the ether oxygen, and TFSI$^-$ coordinating to Li$^+$ is not observed from its Raman spectra.[62] But when x is greater than 2, such side chains worsen the fluidity of the ILs, as well as the electrolytes.[62]

To mitigate the high viscosity, Atik et al. introduced a non-solvating co-solvent, TTE, to CILEs based on LiFSI and Pyr$_{1(2O)71}$FSI.[43] Due to the strong coordination ability of the ether oxygen atoms in the solvating organic cation, i.e.,

Pyr$_{1(2O)71}$$^+$, Li$^+$ in the LCILEs preferentially coordinate to the side chain of the organic cation rather than FSI$^-$, as illustrated in Figure 3c.[43] The influence of the solvating organic cation and the LiFSI concentration on the solvation of Li$^+$ is revealed with Raman spectra as shown in Figure 3d.[43] The addition of TTE does not change the FSI$^-$ local coordination by Li$^+$. Compared with Pyr$_{14}$$^+$, Pyr$_{1(2O)71}$$^+$ leads to a larger amount of free FSI$^-$, due to the coordination of the ether oxygen atoms in Pyr$_{1(2O)71}$$^+$ to Li$^+$. When the LiFSI concentration in Pyr$_{1(2O)71}$FSI:TTE is increased from 0.9 to 1.5 m, the side chains of Pyr$_{1(2O)71}$$^+$ cannot accommodate all the Li$^+$ and FSI$^-$ become involved in Li$^+$ solvation as evidenced by the shift of the peak to higher wavenumbers.[43] This change is accompanied with a decrease of Li$^+$ conductivity at 40 °C from 2.4×10^{-1} to 1.32×10^{-1} mScm^{-1}, demonstrating the impact of the Li$^+$ solvation.[43] It seems the Li$^+$ solvation with organic cations lead to superior Li$^+$ transport, but the rate capability delivered with this LCILE is generally inferior to those with LCILEs employing non-solvating organic cations.[29]

3.2. Interactions between organic cations and anions

Due to the charge delocalisation and/or steric hindrance, the bulky organic cations and anions in most of the ILs for LMBs coordinate weakly. Even though, their interactions have significant influence on the properties of LCILEs, as revealed by a recently reported study evaluating [LiFSI]$_1$[EmimFSI]$_2$[BTFE]$_2$ and [LiFSI]$_1$[Pyr$_{14}$FSI]$_2$[BTFE]$_2$.[48] Compared with the Pyr$_{14}$$^+$-based electrolyte, the Emim$^+$-based electrolyte shows higher ionic conductivity (9.46 vs. 4.02 mScm^{-1}), lower viscosity (41.5 vs. 67.5 mPas), and thoroughly improved Li$^+$ self-diffusion coefficient (3.50×10^{-11} vs. 1.92×10^{-11} m^{2}s^{-1}) at RT. MD simulations revealed similar Li$^+$-FSI$^-$ coordination (identical to Raman spectra) but different interactions between Emim$^+$/Pyr$_{14}$$^+$ and FSI$^-$ in the electrolytes. The average oxygen atoms from FSI$^-$ coordinating to Emim$^+$ and Pyr$_{14}$$^+$ in their first solvation shell is 3.6 and 4.4, respectively, which leads to the different physicochemical properties of the electrolytes.

In fact, the influence of the structures of organic cations and anions on their interactions and physicochemical properties of ILs and ILEs has been investigated thoroughly.[66–69] The reported ionic conductivity, viscosity, and summarised rules are useful for the selection of suitable organic cations and anions for LCILEs. For instance, Borodin et al. have demonstrated that the significant charge delocalisation in Emim$^+$ vs. Pyr$_{13}$$^+$ leads to a lower binding energy of Emim$^+$ towards anions and smaller size of Emim$^+$, which benefits the faster ionic transport and lower viscosity of Emim$^+$-based ILs.[66,67] Specifically, EmimFSI exhibits higher ionic conductivity and lower viscosity than Pyr$_{14}$FSI, which correlates well with the aforementioned LCILEs.[70,71]

3.3. Interactions between organic cations and diluents

The functional interactions between organic cations and the non-solvating diluents were not detected in the early study of LCILEs employing fluorinated ethers as the non-solvating co-solvents. Recently, Lundin et al. reported detailed findings on the ion dynamic and nanostructures of [LiFSI]$_{0.2}$[Pyr$_{14}$FSI]$_1$[TTE]$_x$ (with $x=0$, 0.1, 0.5, and 1).[57] The self-diffusion coefficients of Pyr$_{14}^+$, FSI$^-$, Li$^+$, and TTE in the electrolytes were measured with PFG NMR . As shown in Figure 4a, higher fractions of TTE lead to increased self-diffusion coefficients of all the components, but their rates of increase differ. Particularly, when the self-diffusion coefficients are normalised to the self-diffusion coefficient of Pyr$_{14}^+$ (Figure 4b), the dynamics of Pyr$_{14}^+$ and TTE are evidently correlated, which implies the interaction between them. It is worth noting that the mole ratio of LiFSI to Pyr$_{14}$FSI, i.e., 1:5, is lower than the other reported LCILEs, e.g., 1:2, and even 3:4,[29,30] leading to higher mole fractions of Pyr$_{14}^+$ and "free" FSI$^-$ among the ions. It is anticipated that when the mole ratio of lithium salts to ILs is further increased, the interactions between the organic cations and fluorinated ether co-solvents would be weakened.

In addition, the interaction between the organic cations and diluent molecules can be strengthened by modulating their molecular structure. One typical example is the interaction between Emim$^+$ and dFBn in [LiFSI]$_1$[EmimFSI]$_2$[dFBn]$_2$.[31] Since the positively charged five-membered ring of Emim$^+$ obeys the Hückel rule, Emim$^+$ is 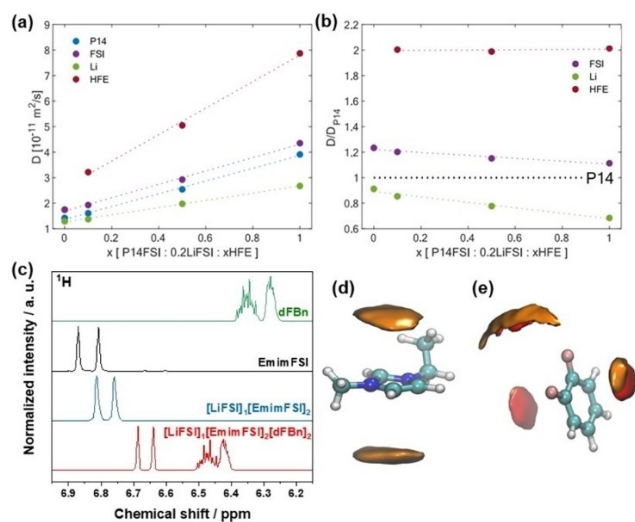aromatic and therefore could transfer part of its positive charge to dFBn via π-π stacking, which is evidenced with the ^{1}H NMR spectra. As shown in Figure 4c, the addition of dFBn to [LiFSI]$_1$[EmimFSI]$_2$ leads to up-field shifts of the peaks of Emim$^+$ (at 6.87 and 6.81 ppm for [LiFSI]$_1$[EmimFSI]$_2$) and down-field shifts of the aromatic peaks of dFBn (6.25–6.40 ppm for neat dFBn). These findings are further corroborated with MD simulations showing the spatial distribution functions around the centres of Emim$^+$ and dFBn. The dFBn (orange distribution clouds) facing the aromatic ring of Emim$^+$ (Figure 4d) and a similar distribution of Emim$^+$ (red clouds) around central dFBn (Figure 4e) evidence how Emim$^+$ and dFBn coordinate to each other. Due to the presence of the slippery π-π stacking interactions, the viscosity of [LiFSI]$_1$[EmimFSI]$_2$[dFBn]$_2$ (24.7 mPa s) is much lower than that of [LiFSI]$_1$[EmimFSI]$_2$[BTFE]$_2$ (41.5 mPa s).[31,48]

4. Electrochemical properties

4.1. LMAs

ILEs based on TFSI$^-$ and particularly FSI$^-$ are known to exhibit high compatibility towards LMAs and enabling dendrite-free cycling of LMAs up to 1000 h, which are, however, based on the relatively low stripping/plating current density, e.g., 0.1 mA cm^{-2}.[14,72] Due to their limited Li$^+$ transport, lithium dendrites still generate during stripping/plating at elevated current densities.[29–31,42,45,46] For example, lithium dendrites are observed in the lithium (1.5 mAh cm^{-2}) deposited on Cu at 0.5 mA cm^{-2} in [LiFSI]$_1$[EmimFSI]$_2$ (Figure 5a).[31] In contrast, dendrite-free morphology of lithium is commonly reported for LCILEs at such current density due to the promoted Li$^+$ transport
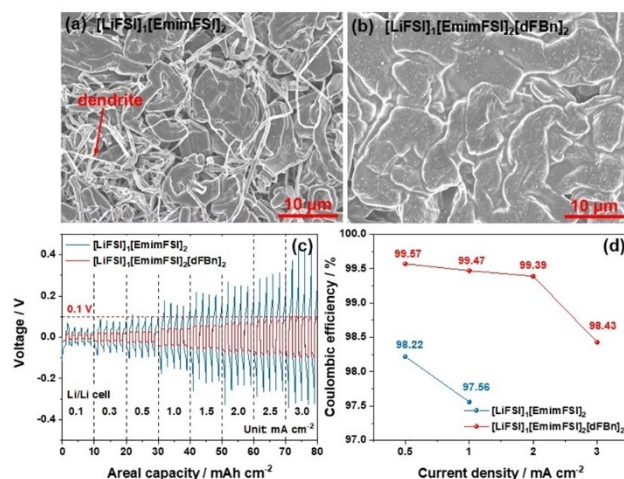

Figure 4. (a) Self-diffusion coefficients of the components of [LiFSI]$_{0.2}$[Pyr$_{14}$FSI]$_1$[TTE]$_x$ determined via PFG NMR at 297 K. (b) Ratio between the self-diffusion coefficients of the components of [LiFSI]$_{0.2}$[Pyr$_{14}$FSI]$_1$[TTE]$_x$ and the self-diffusion coefficient of Pyr$_{14}^+$ cation. (a,b) Adoped from Ref. [57] (c) ^{1}H NMR spectra of dFBn, EmimFSI, [LiFSI]$_1$[EmimFSI]$_2$, and [LiFSI]$_1$[EmimFSI]$_2$[dFBn]$_2$. Spatial distribution functions around the centres of (d) Emim$^+$ and (e) dFBn, respectively, extracted from MD simulation of [LiFSI]$_1$[EmimFSI]$_2$[dFBn]$_2$. The yellow and red clouds represent the dFBn and Emim$^+$. (c–e) Reproduced from Ref. [31].

Figure 5. SEM images of lithium metal (1.5 mAh cm^{-2}) deposited in (a) [LiFSI]$_1$[EmimFSI]$_2$ and (b) [LiFSI]$_1$[EmimFSI]$_2$[dFBn]$_2$ at 0.5 mA cm^{-2}. (c) Voltage profiles of Li plating/stripping processes in Li/Li cells employing either [LiFSI]$_1$[EmimFSI]$_2$ or [LiFSI]$_1$[EmimFSI]$_2$[dFBn]$_2$ at various current densities. (d) Li plating/stripping CE at various current densities in [LiFSI]$_1$[EmimFSI]$_2$ or [LiFSI]$_1$[EmimFSI]$_2$[dFBn]$_2$. (a–d) Adapted from Ref. [31].

(e.g., Figure 5b for [LiFSI]$_1$[EmimFSI]$_2$[dFBn]$_2$).[29,30,41–43,45,46,48]

Moreover, the rate capability and CEs are also promoted by introducing non-solvating co-solvents to CILEs,[30,41–43,45,46] as displayed in Figure 5c,d, for [LiFSI]$_1$[EmimFSI]$_2$ and [LiFSI]$_1$[EmimFSI]$_2$[dFBn]$_2$.[31] Among the reported LCILEs, [LiFSI]$_1$[Pp$_{13}$FSI]$_2$[TTE]$_4$ delivers the best rate capability, allowing stable stripping/plating of Li/Li cells at 10 mA cm^{-2} for 1000 h;[41] the highest lithium stripping/plating CE is 99.72% recorded in [LiFSI]$_1$[EmimFSI]$_2$[mFBn]$_2$.[45] The decent rate capability and reversibility make LCILEs comparable and even superior to various electrolytes based on conventional organic solvents.[34,73–76]

The electrochemical properties are not only promoted by the enhanced Li$^+$ transport ability as introduced in the previous sections but also associated with the SEIs generated on LMAs.[30,31,41,45,46,48] X-ray photoelectron spectroscopy (XPS) is commonly used to characterise the SEIs on LMAs. The SEIs formed on LMAs in ILEs are derived from both organic cations and anions in the electrolytes. The use of different organic cations and anions could change the SEIs,[11–13] and this effect is also observed in LCILEs. For instance, the higher N content of Emim$^+$ with respect to Pyr$_{14}^+$ results in a more stable SEI and consequently higher lithium stripping/plating CE in the LCILEs with the presence of the former cation.[48] It is also noticed that the TFSI$^-$-based LCILEs generally exhibit lower lithium stripping/plating CE than the FSI$^-$-based LCILEs, due to the facile de-fluorination of FSI$^-$.[30,41,42]

In addition, the presence of the fluorinated non-solvating co-solvents could affect the organic cations and anions contribution to the SEI formation, which is usually associated with the promoted lithium stripping/plating CEs.[30,31,41,45] It is commonly reported that the addition of the non-solvating co-solvents leads to the formation of the SEI with fewer organic species, e.g., C–C/C–H, and more inorganic species, e.g., Li$_x$S$_y$ and LiF, which promotes the decomposition of anions, e.g., FSI$^-$ and TFSI$^-$, and suppressed decomposition of organic cations.[30,41,45] Besides, some different effects are also reported. For example, N 1s XPS spectra of the lithium deposited in [LiFSI]$_1$[EmimFSI]$_2$ and [LiFSI]$_1$[EmimFSI]$_2$[dFBn]$_2$ reveal that the signals of positively charged nitrogen atoms from Emim$^+$ (402.1 eV) and negatively charged nitrogen atoms from FSI$^-$ (399.9 eV) are both intensified with the presence of dFBn, indicating more contribution of both Emim$^+$ and FSI$^-$ to the SEI formation.[31] Cai et al. reported similar SEIs generated on LMAs in [LiTFSI]$_{0.8}$[DEMETFSI]$_1$ and [LiTFSI]$_{0.8}$[DEMETFSI]$_1$[OTF]$_4$, demonstrating ignorable influence of OTF on the SEI formation in these electrolytes.[42] Therefore, the effect of the non-solvating co-solvents on the SEI formation depends on the composition of the electrolytes.

4.2. LMBs with insertion-type cathode materials

LiFePO$_4$ (LFP), which possesses high cycling stability and good rate capability, is an ideal model cathode material to investigate the effect of the compatibility between LMAs and developed LCILEs on full cells, as the capacity fading of Li/LFP cells upon cycling can be mainly ascribed to the degradation of LMAs. With the decreased viscosity, promoted Li$^+$ transport ability, and high Li stripping/plating CEs, LCILEs have been reported allowing stable cycling of Li/LFP cells with more practical cathode mass loading, e.g., 9.5 mg cm^{-2}, and dis-/charge current rates, e.g., 1 mA cm^{-2}, for up to hundreds of cycles at RT.[29,41,42,46]

Despite the high cyclability, the energy density of Li/LFP cells is limited by the low tap density, average discharge potential, and specific capacity. Some other types of cathode materials with higher energy density have also been evaluated with LCILEs. Lee et al. reported stable cycling of LiCoO$_2$ (8 mg cm^{-2}) in [LiTFSI]$_1$[Pyr$_{13}$FSI]$_2$[TTE]$_2$ at a dis-/charge current rate of 0.6 mA cm^{-2} over a 3.0–4.3 V voltage range for 350 cycles with a capacity retention of 80%.[30] Nonetheless, the rapidly increasing price of cobalt results in higher cost of LiCoO$_2$-based batteries.[77]

Nickel-rich, layered transition metal oxides (LiNi$_x$Mn$_y$Co$_{1-x-y}$O$_2$, NMC, $x \geq 0.5$) are very promising high-energy and low-cost cathode materials, due to their high specific capacity, high average discharge potential, and possibly low cobalt content.[77] However, increased nickel content usually leads to poor interfacial compatibility toward electrolytes due to the highly reactive Ni^{4+} species generated upon delithiation.[78,79] The parasitic electrolyte degradation results in limited reversibility, thickening of the cathode electrolyte interphase (CEI), and consequently fast capacity fading.[78] A couple of LCILEs enabling stable cycling of LFP for several hundreds of cycles have been employed for Li/LiNi$_x$Mn$_y$Co$_{1-x-y}$O$_2$ ($x = 0.5$ or 0.6) cells; however, they already exhibit pronounced capacity fading after only 100 cycles.[29,43,46] To resolve this issue, Liu et al. designed [LiFSI]$_1$[EmimFSI]$_2$[dFBn]$_2$ for Li/LiNi$_{0.8}$Mn$_{0.1}$Co$_{0.1}$O$_2$ (NMC811) batteries.[31] The preferential decomposition of dFBn limits the decomposition of Emim$^+$ and FSI$^-$ via the generation of LiF-containing CEIs, which leads to less thickening upon cycling with respect to the corresponding CILE, i.e., [LiFSI]$_1$[EmimFSI]$_2$ (Figure 6a–f). As a result, highly stable cycling of Li/NMC811 cells (4.4 V) at C/3 charge and 1 C discharge (1C = 2 mA cm^{-2}) for 500 cycles with a capacity retention of 93% is delivered (Figure 6g). Due to the high lithium stripping/plating CE in this electrolyte, stable cycling up to 250 cycles with a capacity retention of 76% is still achieved when the thick LMAs (100 mAh cm^{-2}) were subsequently replaced with thin LMAs (2 mAh cm^{-2}).

Apart from the inorganic insertion-type cathode materials, the potential use of LCILEs for organic electrode materials has been also demonstrated. Xu et al. reported the use of [LiTFSI]$_{0.101}$[Pyr$_{14}$TFSI]$_{0.274}$[TTE]$_{0.625}$ for Li/3,4,9,10-perylenetetracarboxylic dianhydride (PTCDA) cells.[80] The dissolution of PTCDA during the dis-/charge process in conventional organic electrolytes leads to fast capacity
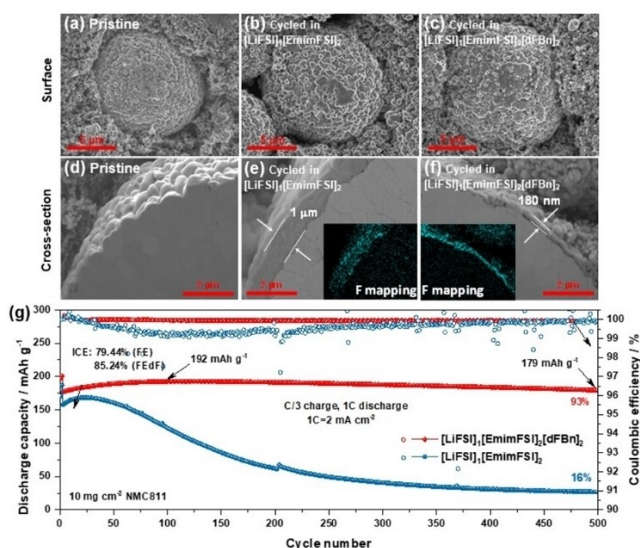
Angew. Chem. Int. Ed. **2023**, *62*, e202219318 (8 of 13)

© 2023 The Authors. Angewandte Chemie International Edition published by Wiley-VCH GmbH

Figure 6. The (a–c) surface and (d–f) cross-sectional morphology of NMC811 particles in the electrodes (a,d) at pristine state, and after 100 cycles in (b,e) [LiFSI]₁[EmimFSI]₂ and (c,f) [LiFSI]₁[EmimFSI]₂[dFBn]₂, respectively. The insets in (e) and (f) display the corresponding energy dispersive X-ray analysis (EDX) elemental mapping images of fluorine. (g) The evolution of discharge specific capacity and CE during long-term cycling of Li/NMC811 cells with NMC811 loading of 10 mg cm⁻² at C/3 charge and 1C discharge after two formation cycles at C/10. (a–g) Adapted from Ref. [31].

fading, but PTCDA, whether at its fully charged or discharged states, is insoluble in both the LCILE and the CILE. The lower viscosity and faster Li⁺ transport of the LCILE with respect to the CILE further promote the specific capacity. As a result, a high capacity of 133 mAh g⁻¹ with a remarkable capacity retention of 99 % after 400 cycles was obtained with the LCILE.

4.3. Li-S batteries

Sulphur, as a low-cost environmental-friendly and abundant substance with a high specific capacity of 1675 mAh g⁻¹, is an appealing cathode material for high-energy density LMBs.[81] Nonetheless, the notorious shuttle effect of polysulphides, i.e., the dissolution and migration of polysulphide, leads to rapid capacity fading and low CE of Li–S batteries.[82–84] With the conventionally used ether-based electrolytes, e.g., 1 M LiTFSI in dimethoxyethane/1,3-dioxolane (DME/DOL), the discharge profile of Li–S batteries shows two plateaus at ≈2.4 and 2.1 V vs. Li/Li⁺, which correspond to the lithiation of long-chain polysulphides and its further transformation to shorter chained polysulphides, eventually Li₂S, respectively.[85] It has been revealed that the solubility of polysulphides, particularly the long-chain ones, in TFSI⁻-based ILEs is suppressed as compared with conventional ether-based electrolytes, which leads to improved cyclability and CE accompanied with when the ILEs are employed.[86,87] Due to the high viscosity and limited Li⁺ transport, the decent specific capacity and cyclability of Li–S cells using

ILEs is realised with low sulphur loading of 0.6 mg cm⁻² and current densities around 0.1 mA cm⁻².[86,87]

In 2018, Lu et al. reported the use of TTE as a co-solvent of LiTFSI-EmimFSI binary ILEs to mitigate the aforementioned issues.[52] The addition of TTE not only resulted in higher ionic conductivity and lower viscosity but also further decreased the solubility of polysulphides (Figure 7a). These improvements of the physicochemical properties enhance the cyclability (Figure 7b) and rate capability with higher sulphur loading (1.5–1.8 mg cm⁻²). The dis-/charge profiles of Li/S cells employing the electrolytes with different contents of TTE are shown in Figure 7c. Due to the sluggish Li⁺ transport, the specific capacity delivered in the neat ILE is low, and the discharge profile does not show any flat voltage plateau. When the LCILEs are employed, the discharge profiles exhibiting a slope around 2.1 V and a plateau slightly below 2.0 V are different from those observed with 1 M LiTFSI in DME/DOL, but similar to those reported from locally concentrated electrolytes based on organic solvents.[85,88] Rebecca et al. recently reported that the difference between the discharge profiles obtained with a conventional ether electrolyte and locally concentrated sulfolane electrolytes originates from a minimised long-chain polysulphides formation with the addition of hydrofluoroether co-solvents in the locally concentrated electrolytes. The poor solubility of Li⁺ in the HFE leads to a shift to favouring short chain length polysulphides in the discharge of sulphur.[85]

Despite the improvement, the relatively rapid capacity fading is still observed in Li–S batteries employing LCILEs.[52,89] In addition to elemental sulphur, sulphurised polyacrylonitrile (SPAN) is a viable alternative.[90–92] The strong interaction between sulphur fragments and dehydrocyclised polyacrylonitrile skeletons suppress the dissolution of polysulphide.[93,94] Particularly, when suitable electrolytes enabling the formation of stable CEIs on SPAN are
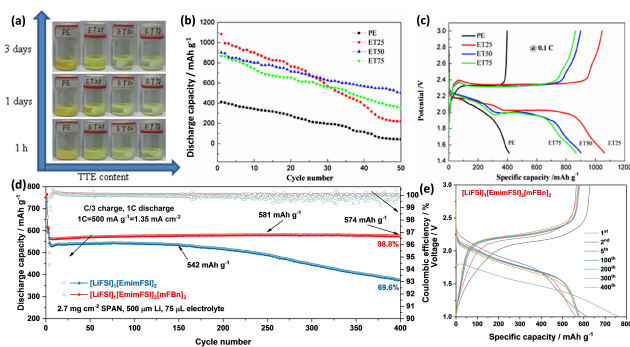

Figure 7. (a) Solubility experiments of polysulphides in 1 M LiTFSI in EmimTFSI-TTE binary solvents. PE, ET25, ET50, and ET75 represent the binary solvents containing 0, 25, 50, 75 wt.% TTE. (b) Cycling performance of Li/S batteries employing electrolytes containing different amounts of TTE. (c) Dis-/charge profiles of Li/S cells employing electrolytes containing different amounts of TTE. (a–c) Adapted from Ref. [52] (d) Evolution of discharge capacity and CE of Li/SPAN cells employing [LiFSI]₁[EmimFSI]₂[mFBn]₂ upon cycling at C/3 charge and 1C discharge after three formation cycles at C/10, and (e) corresponding dis-/charge profiles (Reproduced from Ref. [45]).

employed, e.g., carbonate-based electrolytes, a solid-phase mechanism with negligible polysulphide dissolution can be realised leading to stable cycling up to hundreds of cycles.[95,96] Liu et al. reported the good compatibility of $[LiFSI]_1[EmimFSI]_2$ and $[LiFSI]_1[EmimFSI]_2[mFBn]_2$ with the SPAN cathodes (Figure 7d), due to the formation of protective CEI derived mainly from FSI^- and $Emim^+$.[45] As shown in Figure 7e, the dis-/charge profiles of the Li/SPAN cell employing $[LiFSI]_1[EmimFSI]_2[mFBn]_2$ as the electrolyte do not show any flat voltage plateau, demonstrating that no phase transition is involved in the dis-/charge, i.e., a solid-like phase mechanism occurs. Because of the higher lithium stripping/plating CE in the presence of mFBn, the LCILE leads to better cyclability with respect to the neat ILE. Benefiting from the robust interphases simultaneously formed on both LMAs and SPAN cathodes, highly stable cycling of Li/SPAN cells (80% lithium metal excess) for 250 cycles with a capacity retention of 71% is achieved employing $[LiFSI]_1[EmimFSI]_2[mFBn]_2$.

4.4. Li-O₂ batteries

Li-O₂ batteries are propitious energy storage candidates for the next generation high-energy-density batteries, yet their development is limited by several exigent challenges.[97] Among them, the instability of their electrolytes exposed to highly reactive $O_2^{-\bullet}$ intermediates formed during the electrochemical process is considered the most serious one.[98,99] $TFSI^-$-based ILEs, exhibiting modest reactivity with the $O_2^{-\bullet}$, are one of the few electrolytes enabling reversible Li-O₂ batteries.[100–102] However, the insufficient lithium stripping/plating CE and Li^+ transport ability of the ILEs result in limited lifespan and high polarisation of the ILEs-based Li-O₂ batteries.[100–102] In 2021, Cai et al. reported the use of the optimised LCILE, i.e., $[LiTFSI]_{0.8}[DEMETFSI]_1[OTF]_4$, for Li-O₂ batteries.[41] Due to the improved reversibility of LMAs and promoted Li^+ transportability with the presence of the OTF co-solvent, the overvoltage and cyclability are significantly improved (Figure 8). With differential electrochemical mass spectrometry, XPS, and acid-base titration, the discharge product was revealed to be Li_2O_2.

5. Conclusion and Outlook

The non-flammable nature, dendrite-free LMAs with high CE, and good cyclability of various high-energy cathode materials in the rationally designed LCILEs suggest their promising application in the next-generation (safe) high-energy-density LMBs. The addition of non-solvating fluorinated co-solvents to ILEs not only mitigates their drawbacks of insufficient fluidity, wettability, and Li^+ transport, but also promotes their compatibility toward LMAs, which represents the remarkable progress of ILEs in the battery field. In addition, the role of organic cations, anions, and non-solvating co-solvents in relation to how they distribute and interact in LCILEs has been studied illustrating that all
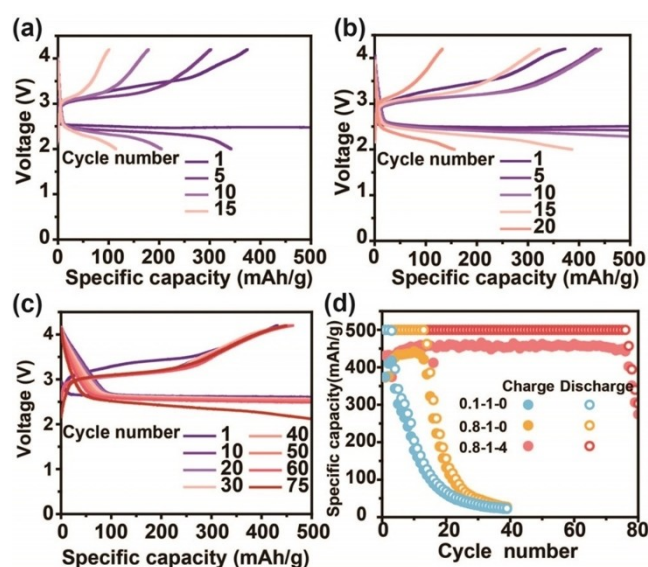

Figure 8. Discharge-charge voltage profiles of the Li-O₂ cells employing (a) $[LiTFSI]_{0.1}[DEMETFSI]_1$, (b) $[LiTFSI]_{0.8}[DEMETFSI]_1$, and (c) $[LiTFSI]_{0.8}[DEMETFSI]_1[OTF]_4$. (d) The comparison of charge/discharge capacity of Li-O₂ cells employing these electrolytes. (a–d) Adapted from Ref. [41].

the components (including electrolyte solution structures) have an influence on the physicochemical properties. Despite recent advancements, LCILEs are still in their infancy with collaborations across disciplines utilising theoretical, experimental, and advanced characterisation techniques requisite to further understanding and enhance cell performance.

Optimisation of LCILEs for superior battery performance is one of the core directions for further investigation of LCILEs, which includes selecting suitable electrolyte components and adjusting their concentrations. Different electrode materials manifest distinct interactions with electrolytes, imposing diverse requirements on the electrolytes. Therefore, the optimisation of advanced LCILEs depends on the specific cathode material, while considering the compatibility toward LMAs. Previous studies on the application of ILEs for different cathode chemistry for LMBs is insightful for the primary selection of organic cations and anions for LCILEs. Nonetheless, it is probable that the addition of non-solvating co-solvent may alter the findings of the study of ILEs via participating/affecting the formation of electrolyte/electrode interphases (EEIs). For example, Pyr_{14}^+ is more stable than $Emim^+$ toward LMAs in ILEs,[71] but the $Emim^+$-based LCILE shows improved lithium stripping/plating CE.[48] Therefore, revisiting the vast choices of organic cations and anions is expected to result in interesting outcomes that can inform on the design of ILEs. The ratio of lithium salts, ILs, and co-solvents has significant influence on the viscosity, Li^+ transport, and EEI formation. The enhancement of these electrolytic mediums relies on balancing these properties. However, current cells are studied/operated in far from practical conditions. Further development of electrolyte formulas for the cells under

operando conditions, e.g., Ah-level cells with high areal capacity, lean electrolyte, and low negative/positive (N/P) ratio, are essential to attain practical application.

Apart from the electrolyte optimisation, studies exploring the electrolyte structure, dynamics and mechanisms as well as how their concentrations affect the electrolytes' physicochemical properties and EEI formation is equally important as this will guide the rational engineering of stable mediums. Although some physical determinations of LCILEs' solution structure have been obtained, how the mole ratio of lithium salts, organic cations, and co-solvents affect the ion-ion and ion-solvent interactions remains unknown. The strong interactions between Li^+ and anions can be sensitively characterised using Raman spectroscopy, but this is not the case for the weaker interactions, e.g., organic cations-solvents, and particularly, organic cations-anions. NMR can provide some insights, yet the observed signals need the support of theoretical methods including MD simulations to offer complementary explanations. Importantly, the rate capability of LMBs is not only influenced by the Li^+ transport in the bulk electrolyte, but also the Li^+ transport across the electrode/electrolyte interface/interphase. The former is intensively studied and its relation to the solution structure has gained some important insights, while the interfacial/interphasial Li^+ transport is much less understood. Further experimental and computational efforts to discriminate the respective contribution of the bulk and interfacial resistance, and to understand the interfacial transport process, including the de-/solvation process of Li^+ and $Li^{+'}$ migration across the EEIs, are required and could further promote the rate capability of the LMBs employing LCILEs. In addition, the difference of Li^+ solvation in LCILEs and their corresponding CILEs is very limited, but the resultant generated EEIs are likely unique. In this context, the combination of theoretical methods (e.g., density functional theory and ab initio molecular dynamics) and experimental techniques (e.g., XPS, differential electrochemical mass spectrometry, soft X-ray adsorption spectroscopy) can be utilised. Computational approaches that describe the complete electronic structure at the atomic scale can explicate the intricate interactions (including van der Waals, dispersion, hydrogen bonding, etc.,) of LCILEs. The results can be made more intelligible when used in synergy with operando experiments such as neutron scattering which utilise non-destructive probes with high material penetration depth offering energy/frequency range along with spatial-temporal resolution. The formation, composition and evolution of interfacial dynamical processes at the EEI can be captured utilising in situ neutron scattering techniques (quasi-elastic, inelastic, etc.,) which are sensitive to light elements (H & Li). Towards real-time determinations of LCILEs under operating conditions, neutrons could probe the relationship between structure and electrochemical performance in battery materials under operation. Such methodologies that combine theoretical and advanced experimental techniques will elucidate the functional behaviour of LCILEs for the development of the next generation high-energy-density LMBs.

Author Contributions

X.L.: Conceptualization (lead); Project administration (lead); Writing-original draft (lead); Writing-review & editing (supporting). A.M.: Writing-original draft (supporting); Writing-review & editing (supporting). H.A.: Writing-review & editing (equal). S.P.: Conceptualization (equal); Funding acquisition (lead); Resources (lead); Supervision (lead); Writing-review & editing (lead).

Conflict of Interest

The authors declare no conflict of interest.

[1] X. He, D. Bresser, S. Passerini, F. Baakes, U. Krewer, J. Lopez, C. T. Mallia, Y. Shao-Horn, I. Cekic-Laskovic, S. Wiemers-Meyer, F. A. Soto, V. Ponce, J. M. Seminario, P. B. Balbuena, H. Jia, W. Xu, Y. Xu, C. Wang, B. Horstmann, R. Amine, C. C. Su, J. Shi, K. Amine, M. Winter, A. Latz, R. Kostecki, *Nat. Rev. Mater.* **2021**, *6*, 1036–1052.

[2] G. M. Hobold, J. Lopez, R. Guo, N. Minafra, A. Banerjee, Y. Shirley Meng, Y. Shao-Horn, B. M. Gallant, *Nat. Energy* **2021**, *6*, 951–960.

[3] J. Wang, L. Li, H. Hu, H. Hu, Q. Guan, M. Huang, L. Jia, H. Adenusi, K. V. Tian, J. Zhang, S. Passerini, H. Lin, *ACS Nano* **2022**, *16*, 17729–17760.

[4] G. Xu, L. Huang, C. Lu, X. Zhou, G. Cui, *Energy Storage Mater.* **2020**, *31*, 72–86.

[5] Y. Wu, X. Feng, M. Yang, C. Z. Zhao, X. Liu, D. Ren, Z. Ma, L. Lu, L. Wang, G. L. Xu, X. He, K. Amine, M. Ouyang, *Adv. Sci.* **2022**, *9*, 2204059.

[6] J. G. Zhang, W. Xu, J. Xiao, X. Cao, J. Liu, *Chem. Rev.* **2020**, *120*, 13312–13348.

[7] W.-Y. Kim, H.-I. Kim, K. M. Lee, E. Shin, X. Liu, H. Moon, H. Adenusi, S. Passerini, S. K. Kwak, S.-Y. Lee, *Energy Environ. Sci.* **2022**, *15*, 5217–5228.

[8] D. R. MacFarlane, M. Forsyth, P. C. Howlett, M. Kar, S. Passerini, J. M. Pringle, H. Ohno, M. Watanabe, F. Yan, W. Zheng, S. Zhang, J. Zhang, *Nat. Rev. Mater.* **2016**, *1*, 15005.

[9] X. Tang, S. Lv, K. Jiang, G. Zhou, X. Liu, *J. Power Sources* **2022**, *542*, 231792.

[10] J. Kalhoff, G. G. Eshetu, D. Bresser, S. Passerini, *ChemSusChem* **2015**, *8*, 2154–2175.

[11] Y. Preibisch, F. Horsthemke, M. Winter, S. Nowak, A. S. Best, *Chem. Mater.* **2020**, *32*, 2389–2398.

[12] M. Olschewski, R. Gustus, O. Höfft, A. Lahiri, F. Endres, *J. Phys. Chem. C* **2017**, *121*, 2675–2682.

[13] K. Periyapperuma, E. Arca, S. Harvey, C. Ban, A. Burrell, D. R. Macfarlane, C. Pozo-Gonzalo, M. Forsyth, P. C. Howlett, *J. Mater. Chem. A* **2020**, *8*, 3574–3579.

[14] F. Wu, S. Fang, M. Kuenzel, A. Mullaliu, J. K. Kim, X. Gao, T. Diemant, G. T. Kim, S. Passerini, *Joule* **2021**, *5*, 2177–2194.

[15] P. Liang, H. Sun, C. Huang, G. Zhu, H. Tai, J. Li, F. Wang, Y. Wang, C. Huang, S. Jiang, M. Lin, Y. Li, B. Hwang, C. Wang, H. Dai, *Adv. Mater.* **2022**, *34*, 2207361.

[16] F. Wu, G. T. Kim, T. Diemant, M. Kuenzel, A. R. Schür, X. Gao, B. Qin, D. Alwast, Z. Jusys, R. J. Behm, D. Geiger, U. Kaiser, S. Passerini, *Adv. Energy Mater.* **2020**, *10*, 2001830.

[17] J. P. Brinkmann, N. Ehteshami-Flammer, M. Luo, M. Leißing, S. Röser, S. Nowak, Y. Yang, M. Winter, J. Li, *ACS Appl. Energy Mater.* **2021**, *4*, 10909–10920.

[18] Y. Peng, R. Badam, T. P. Jayakumar, W. Wannapakdee, C. Changtong, N. Matsumi, *J. Electrochem. Soc.* **2022**, *169*, 050515.

[19] U. Ulissi, G. A. Elia, S. Jeong, J. Reiter, N. Tsiouvaras, S. Passerini, J. Hassoun, *Chem. Eur. J.* **2018**, *24*, 3178–3185.

[20] A. Heist, S.-H. Lee, *J. Electrochem. Soc.* **2019**, *166*, A1677.

[21] G. A. Giffin, A. Moretti, S. Jeong, K. Pilar, M. Brinkkötter, S. G. Greenbaum, M. Schönhoff, S. Passerini, *ChemSusChem* **2018**, *11*, 1981–1989.

[22] X. Gao, F. Wu, A. Mariani, S. Passerini, *ChemSusChem* **2019**, *12*, 4185–4193.

[23] H. Yoon, A. S. Best, M. Forsyth, D. R. MacFarlane, P. C. Howlett, *Phys. Chem. Chem. Phys.* **2015**, *17*, 4656–4663.

[24] H. Sun, G. Zhu, Y. Zhu, M. C. Lin, H. Chen, Y. Y. Li, W. H. Hung, B. Zhou, X. Wang, Y. Bai, M. Gu, C. L. Huang, H. C. Tai, X. Xu, M. Angell, J. J. Shyue, H. Dai, *Adv. Mater.* **2020**, *32*, 2001741.

[25] Q. J. Meisner, T. Rojas, T. Glossmann, A. Hintennach, Q. Liu, J. Cao, P. C. Redfern, A. T. Ngo, L. A. Curtiss, Z. Zhang, *J. Electrochem. Soc.* **2020**, *167*, 070528.

[26] U. Pal, F. Chen, D. Gyabang, T. Pathirana, B. Roy, R. Kerr, D. R. MacFarlane, M. Armand, P. C. Howlett, M. Forsyth, *J. Mater. Chem. A* **2020**, *8*, 18826–18839.

[27] U. Pal, D. Rakov, B. Lu, B. Sayahpour, F. Chen, B. Roy, D. R. MacFarlane, M. Armand, P. C. Howlett, Y. S. Meng, M. Forsyth, *Energy Environ. Sci.* **2022**, *15*, 1907–1919.

[28] R. S. Kühnel, N. Böckenfeld, S. Passerini, M. Winter, A. Balducci, *Electrochim. Acta* **2011**, *56*, 4092–4099.

[29] X. Liu, M. Zarrabeitia, A. Mariani, X. Gao, H. M. Schütz, S. Fang, T. Bizien, G. A. Elia, S. Passerini, *Small Methods* **2021**, *5*, 2100168.

[30] S. Lee, K. Park, B. Koo, C. Park, M. Jang, H. Lee, H. Lee, *Adv. Funct. Mater.* **2020**, *30*, 2003132.

[31] X. Liu, A. Mariani, T. Diemant, M. E. Di Pietro, X. Dong, M. Kuenzel, A. Mele, S. Passerini, *Adv. Energy Mater.* **2022**, *12*, 2200862.

[32] X. Cao, H. Jia, W. Xu, J.-G. Zhang, *J. Electrochem. Soc.* **2021**, *168*, 010522.

[33] S. Chen, J. Zheng, D. Mei, K. S. Han, M. H. Engelhard, W. Zhao, W. Xu, J. Liu, J. G. Zhang, *Adv. Mater.* **2018**, *30*, 1706102.

[34] S. Chen, J. Zheng, L. Yu, X. Ren, M. H. Engelhard, C. Niu, H. Lee, W. Xu, J. Xiao, J. Liu, J. G. Zhang, *Joule* **2018**, *2*, 1548–1558.

[35] N. Piao, X. Ji, H. Xu, X. Fan, L. Chen, S. Liu, M. N. Garaga, S. G. Greenbaum, L. Wang, C. Wang, X. He, *Adv. Energy Mater.* **2020**, *10*, 1903568.

[36] X. Ren, L. Zou, X. Cao, M. H. Engelhard, W. Liu, S. D. Burton, H. Lee, C. Niu, B. E. Matthews, Z. Zhu, C. Wang, B. W. Arey, J. Xiao, J. Liu, J. G. Zhang, W. Xu, *Joule* **2019**, *3*, 1662–1676.

[37] G. Zhang, X. Deng, J. Li, J. Wang, G. Shi, Y. Yang, J. Chang, K. Yu, S. Sen Chi, H. Wang, P. Wang, Z. Liu, Y. Gao, Z. Zheng, Y. Deng, C. Wang, *Nano Energy* **2022**, *95*, 107014.

[38] X. Cao, L. Zou, B. E. Matthews, L. Zhang, X. He, X. Ren, M. H. Engelhard, S. D. Burton, P. Z. El-Khoury, H. S. Lim, C. Niu, H. Lee, C. Wang, B. W. Arey, C. Wang, J. Xiao, J. Liu, W. Xu, J. G. Zhang, *Energy Storage Mater.* **2021**, *34*, 76–84.

[39] Z. Jiang, Z. Zeng, X. Liang, L. Yang, W. Hu, C. Zhang, Z. Han, J. Feng, J. Xie, *Adv. Funct. Mater.* **2021**, *31*, 2005991.

[40] D. J. Yoo, S. Yang, K. J. Kim, J. W. Choi, *Angew. Chem. Int. Ed.* **2020**, *59*, 14869–14876; *Angew. Chem.* **2020**, *132*, 14979–14986.

[41] Z. Wang, F. Zhang, Y. Sun, L. Zheng, Y. Shen, D. Fu, W. Li, A. Pan, L. Wang, J. Xu, J. Hu, X. Wu, *Adv. Energy Mater.* **2021**, *11*, 2003752.

[42] Y. Cai, Q. Zhang, Y. Lu, Z. Hao, Y. Ni, J. Chen, *Angew. Chem. Int. Ed.* **2021**, *60*, 25973–26184; *Angew. Chem.* **2021**, *133*, 26177–26184.

[43] J. Atik, M. Winter, E. Paillard, *Electrochim. Acta* **2022**, *415*, 140181.

[44] Z. Wang, H. Zhang, R. Han, J. Xu, A. Pan, F. Zhang, D. Huang, Y. Wei, L. Wang, H. Song, Y. Liu, Y. Shen, J. Hu, X. Wu, *ACS Sustainable Chem. Eng.* **2022**, *10*, 12023–12029.

[45] X. Liu, T. Diemant, A. Mariani, X. Dong, M. E. Di Pietro, A. Mele, S. Passerini, *Adv. Mater.* **2022**, *34*, 2207155.

[46] H. Tu, L. Li, Z. Wang, J. Wang, H. Lin, M. Wang, C. Yan, M. Liu, *ACS Nano* **2022**, *16*, 16898–16908.

[47] X. Ren, S. Chen, H. Lee, D. Mei, M. H. Engelhard, S. D. Burton, W. Zhao, J. Zheng, Q. Li, M. S. Ding, M. Schroeder, J. Alvarado, K. Xu, Y. S. Meng, J. Liu, J. G. Zhang, W. Xu, *Chem* **2018**, *4*, 1877–1892.

[48] X. Liu, A. Mariani, M. Zarrabeitia, M. E. Di Pietro, X. Dong, G. A. Elia, A. Mele, S. Passerini, *Energy Storage Mater.* **2022**, *44*, 370–378.

[49] Y. Zou, Z. Ma, G. Liu, Q. Li, D. Yin, X. Shi, Z. Cao, Z. Tian, H. Kim, Y. Guo, C. Sun, L. Cavallo, L. Wang, H. N. Alshareef, Y. K. Sun, J. Ming, *Angew. Chem. Int. Ed.* **2022**, *61*, e202216189; *Angew. Chem.* **2022**, *134*, e202216189.

[50] Q. Sun, Z. Cao, Z. Ma, J. Zhang, H. Cheng, X. Guo, G. T. Park, Q. Li, E. Xie, L. Cavallo, Y. K. Sun, J. Ming, *ACS Energy Lett.* **2022**, *7*, 3545–3556.

[51] W. Wahyudi, X. Guo, V. Ladelta, L. Tsetseris, M. I. Nugraha, Y. Lin, V. Tung, N. Hadjichristidis, Q. Li, K. Xu, J. Ming, T. D. Anthopoulos, *Adv. Sci.* **2022**, *9*, 2202405.

[52] H. Lu, Z. Chen, H. Du, K. Zhang, J. Wang, Z. Hou, J. Fang, *Ionics* **2019**, *25*, 2685–2691.

[53] American Occupational Safety and Health Standards, from https://www.osha.gov/laws-regs/regulations/standardnumber/1910/1910.106 (accessed: January 2023).

[54] M. Kirchhöfer, J. Von Zamory, E. Paillard, S. Passerini, *Int. J. Mol. Sci.* **2014**, *15*, 14868–14890.

[55] C. F. J. Francis, I. L. Kyratzis, A. S. Best, *Adv. Mater.* **2020**, *32*, 1904205.

[56] K. Xu, *Commun. Mater.* **2022**, *3*, 31.

[57] F. Lundin, A. Idström, P. Falus, L. Evenäs, S. Xiong, A. Matic, *J. Phys. Chem. C* **2022**, *126*, 16262–16271.

[58] Q. Sun, Z. Cao, Z. Ma, J. Zhang, W. Wahyudi, G. Liu, H. Cheng, T. Cai, E. Xie, L. Cavallo, Q. Li, J. Ming, *Adv. Funct. Mater.* **2023**, *33*, 2210292.

[59] H. Cheng, Q. Sun, L. Li, Y. Zou, Y. Wang, T. Cai, F. Zhao, G. Liu, Z. Ma, W. Wahyudi, Q. Li, J. Ming, *ACS Energy Lett.* **2022**, *7*, 490–513.

[60] Y. Zou, Z. Cao, J. Zhang, W. Wahyudi, Y. Wu, G. Liu, Q. Li, H. Cheng, D. Zhang, G. T. Park, L. Cavallo, T. D. Anthopoulos, L. Wang, Y. K. Sun, J. Ming, *Adv. Mater.* **2021**, *33*, 2102964.

[61] Z. Wang, H. Zhang, J. Xu, A. Pan, F. Zhang, L. Wang, R. Han, J. Hu, M. Liu, X. Wu, *Adv. Funct. Mater.* **2022**, *32*, 2112598.

[62] J. Von Zamory, G. A. Giffin, S. Jeremias, F. Castiglione, A. Mele, E. Paillard, S. Passerini, *Phys. Chem. Chem. Phys.* **2016**, *18*, 21539–21547.

[63] J. Atik, D. Diddens, J. H. Thienenkamp, G. Brunklaus, M. Winter, E. Paillard, *Angew. Chem. Int. Ed.* **2021**, *60*, 11919–11927; *Angew. Chem.* **2021**, *133*, 12026–12034.

[64] P. Nürnberg, J. Atik, O. Borodin, M. Winter, E. Paillard, M. Schönhoff, *J. Am. Chem. Soc.* **2022**, *144*, 4657–4666.

[65] M. Kunze, E. Paillard, S. Jeong, G. B. Appetecchi, M. Schoönhoff, M. Winter, S. Passerini, *J. Phys. Chem. C* **2011**, *115*, 19431–19436.

[66] O. Borodin, W. Gorecki, G. D. Smith, M. Armand, *J. Phys. Chem. B* **2010**, *114*, 6786–6798.

[67] O. Borodin, *J. Phys. Chem. B* **2009**, *113*, 12353–12357.

[68] H. Tokuda, K. Hayamizu, K. Ishii, M. A. B. H. Susan, M. Watanabe, *J. Phys. Chem. B* **2004**, *108*, 16593–16600.

[69] H. Tokuda, K. Hayamizu, K. Ishii, M. A. B. H. Susan, M. Watanabe, *J. Phys. Chem. B* **2005**, *109*, 6103–6110.

[70] Q. Zhou, W. A. Henderson, G. B. Appetecchi, M. Montanino, S. Passerini, *J. Phys. Chem. B* **2008**, *112*, 13577–13580.

[71] H. Matsumoto, H. Sakaebe, K. Tatsumi, M. Kikuta, E. Ishiko, M. Kono, *J. Power Sources* **2006**, *160*, 1308–1313.

[72] G. A. Elia, U. Ulissi, S. Jeong, S. Passerini, J. Hassoun, *Energy Environ. Sci.* **2016**, *9*, 3210–3220.

[73] S. Liu, J. Ji, N. Piao, J. Chen, N. Eidson, J. Xu, P. Wang, L. Chen, J. Zhang, T. Deng, S. Hou, T. Jin, H. Wan, J. Li, J. Tu, C. Wang, *Angew. Chem. Int. Ed.* **2021**, *60*, 3661–3671; *Angew. Chem.* **2021**, *133*, 3705–3715.

[74] J. Fu, X. Ji, J. Chen, L. Chen, X. Fan, D. Mu, C. Wang, *Angew. Chem. Int. Ed.* **2020**, *59*, 22194; *Angew. Chem.* **2020**, *132*, 22378.

[75] Y. Huang, R. Li, S. Weng, H. Zhang, C. Zhu, D. Lu, C. Sun, X. Huang, T. Deng, L. Fan, L. Chen, X. Wang, X. Fan, *Energy Environ. Sci.* **2022**, *15*, 4349–4361.

[76] C. Zhu, C. Sun, R. Li, S. Weng, L. Fan, X. Wang, L. Chen, M. Noked, X. Fan, *ACS Energy Lett.* **2022**, *7*, 1338–1347.

[77] W. Li, E. M. Erickson, A. Manthiram, *Nat. Energy* **2020**, *5*, 26–34.

[78] X. Fan, C. Wang, *Chem. Soc. Rev.* **2021**, *50*, 10486–10566.

[79] N. Voronina, Y. K. Sun, S. T. Myung, *ACS Energy Lett.* **2020**, *5*, 1814–1824.

[80] T. Xu, J. Qin, J. Liu, Q. Lan, Y. Zhao, Z. Song, H. Zhan, *ChemElectroChem* **2021**, *8*, 4625–4632.

[81] M. Wang, Z. Bai, T. Yang, C. Nie, X. Xu, Y. Wang, J. Yang, S. Dou, N. Wang, *Adv. Energy Mater.* **2022**, *12*, 2201585.

[82] L. Wang, Y. Ye, N. Chen, Y. Huang, L. Li, F. Wu, R. Chen, *Adv. Funct. Mater.* **2018**, *28*, 1800919.

[83] W. P. Wang, J. Zhang, J. Chou, Y. X. Yin, Y. You, S. Xin, Y. G. Guo, *Adv. Energy Mater.* **2021**, *11*, 2000791.

[84] G. Di Donato, T. Ates, H. Adenusi, A. Varzi, M. A. Navarra, S. Passerini, *Batteries Supercaps* **2022**, *5*, e202200097.

[85] R. Glaser, O. Borodin, B. Johnson, S. Jhulki, G. Yushin, *J. Electrochem. Soc.* **2021**, *168*, 090543.

[86] J. W. Park, K. Yamauchi, E. Takashima, N. Tachikawa, K. Ueno, K. Dokko, M. Watanabe, *J. Phys. Chem. C* **2013**, *117*, 4431–4440.

[87] J. W. Park, K. Ueno, N. Tachikawa, K. Dokko, M. Watanabe, *J. Phys. Chem. C* **2013**, *117*, 20531–20541.

[88] J. Zheng, G. Ji, X. Fan, J. Chen, Q. Li, H. Wang, Y. Yang, K. C. DeMella, S. R. Raghavan, C. Wang, *Adv. Energy Mater.* **2019**, *9*, 1803774.

[89] H. Lu, Z. Chen, Y. Yuan, H. Du, J. Wang, X. Liu, Z. Hou, K. Zhang, J. Fang, Y. Qu, *J. Electrochem. Soc.* **2019**, *166*, A2453.

[90] J. Wang, J. Yang, J. Xie, N. Xu, *Adv. Mater.* **2002**, *14*, 963.

[91] M. S. Ahmed, S. Lee, M. Agostini, M. G. Jeong, H. G. Jung, J. Ming, Y. K. Sun, J. Kim, J. Y. Hwang, *Adv. Sci.* **2021**, *8*, 2101123.

[92] H. Yang, J. Chen, J. Yang, J. Wang, *Angew. Chem. Int. Ed.* **2020**, *59*, 7306–7318; *Angew. Chem.* **2020**, *132*, 7374–7386.

[93] J. Chen, H. Lu, X. Zhang, Y. Zhang, J. Yang, Y. Nuli, Y. Huang, J. Wang, *Energy Storage Mater.* **2022**, *50*, 387–394.

[94] B. He, Z. Rao, Z. Cheng, D. Liu, D. He, J. Chen, Z. Miao, L. Yuan, Z. Li, Y. Huang, *Adv. Energy Mater.* **2021**, *11*, 2003690.

[95] Z. Shen, W. Zhang, S. Mao, S. Li, X. Wang, Y. Lu, *ACS Energy Lett.* **2021**, *6*, 2673–2681.

[96] W. Wang, Z. Cao, G. A. Elia, Y. Wu, W. Wahyudi, E. Abou-Hamad, A. H. Emwas, L. Cavallo, L. J. Li, J. Ming, *ACS Energy Lett.* **2018**, *3*, 2899–2907.

[97] L. Grande, E. Paillard, J. Hassoun, J. B. Park, Y. J. Lee, Y. K. Sun, S. Passerini, B. Scrosati, *Adv. Mater.* **2015**, *27*, 784.

[98] W. J. Kwak, S. Chae, R. Feng, P. Gao, J. Read, M. H. Engelhard, L. Zhong, W. Xu, J. G. Zhang, *ACS Energy Lett.* **2020**, *5*, 2182–2190.

[99] W. J. Kwak, H. S. Lim, P. Gao, R. Feng, S. Chae, L. Zhong, J. Read, M. H. Engelhard, W. Xu, J. G. Zhang, *Adv. Funct. Mater.* **2021**, *31*, 2002927.

[100] U. Ulissi, G. A. Elia, S. Jeong, F. Mueller, J. Reiter, N. Tsiouvaras, Y. K. Sun, B. Scrosati, S. Passerini, J. Hassoun, *ChemSusChem* **2018**, *11*, 229–236.

[101] G. A. Elia, J. Hassoun, W. J. Kwak, Y. K. Sun, B. Scrosati, F. Mueller, D. Bresser, S. Passerini, P. Oberhumer, N. Tsiouvaras, J. Reiter, *Nano Lett.* **2014**, *14*, 6572–6577.

[102] L. Grande, E. Paillard, G. T. Kim, S. Monaco, S. Passerini, *Int. J. Mol. Sci.* **2014**, *15*, 8122–8137.